Advances in Science and Technology Research Journal

Advances in Science and Technology Research Journal 2023, 17(5), 302–312
https://doi.org/10.12913/22998624/172749
ISSN 2299-8624, License CC-BY 4.0

Received: 2023.08.16
Accepted: 2023.09.21
Published: 2023.10.20

Investigate the Metallurgical, Degradation Behaviour, and Mechanical Characteristics of Mg-2Al-1Nd: Novel Magnesium Alloy

Baraa H. Al Khaqani[1*], Nawal Mohammed Dawood[1]

[1] College of Materials Engineering, University of Babylon, Iraq
* Corresponding author's email: baraaalkhaqani@gmail.com

ABSTRACT

Today, the use of magnesium alloys in medical applications as a decomposing material is extensive, so a new magnesium alloy Mg-2Al-1Nd was prepared by an investment-casting method in a medium protected from atmospheric oxygen. One of the rare elements, Nd, was added to improve the microstructural and mechanical properties and corrosion resistance in simulated blood plasma media. The XRF test determined the chemical characterization elements, the SEM test was used to identify the distribution of phases and their shape inside the base before and after heat treatment, and the XRD test was conducted to determine the type of phases that formed and the effect of these phases on other properties was studied. Also, hardness was measured using Vickers microhardness, in which the improvement rate was 75%, and a compression test to determine the mechanical properties of the prepared alloy found that the modulus of elasticity was 42 GPa. To study its corrosive behavior inside the human body, a test was conducted on corrosion by the Tafel method to measure corrosion resistance in simulated blood plasma solution, Where the value of the corrosion rate of the alloy after the heat treatment became 0.089 mm/y and Rp equal 4.13 kΩ/cm^2, These results made the new magnesium alloy a good candidate for use in temporary medical applications.

Keywords: magnesium, biodegradable alloys, rare earth, biomedical application, corrosion resistance.

INTRODUCTION

Mg-alloys are the significantly lightest construction metals that have attracted interest in recent years owing to their enormous scope for application in the automobile and aerospace fields [1, 2]. Additionally, magnesium alloys are interesting choices for orthopaedic surgical applications for a novel type of biodegradable implants owing to their biodegradability, bio-compatibility, and mechanical properties similar to normal bone [3]. Nevertheless, the majority of the alloys being researched today for use in medical fields were adapted to commercial Magnesium alloys, all of which were initially created for engineering applications [4, 5]. Aluminum (Al) and rare earth elements (REE), for instance, are present in the compounds AZ91, WE43, and LAE442. Al has been contentiously blamed for contributing to Alzheimer's disease. Additionally, it might prevent the production of ATP and phosphorylation, decreasing the body's internal energy stored. Evidence that aluminium intake may cause excessive inflammation activity within the brain is supported by epidemiological research [6, 7]. On the other hand, REE (rare earth elements) have raised concerns because they are not normally found in humans' bodies. Prospective studies have been proposed to assess the long-term effects of REE exposures [8]. It makes sense from this perspective to ensure the biological safety of implantation materials to choose alloying elements for the mg-a matrix with minimal adverse effects. Due to its unique qualities, such as reduced density, high specific resistance, and outstanding cast ability, mg finds extensive use in the automotive and aerospace industries. Due to its tolerable corrosive behaviour and moderate toxicity, all these characteristics have prompted researchers to explore the potential for employing magnesium in

medical applications for biodegradable bodies [1, 2]. The phases produced by aluminium and rare earth elements (Al-RE), whereby the Al11RE3 phase forms, are linked to an enhancement in the creep resistance of the Mg-Al-RE alloy known as AZ91 when combined with the standard Mg-Al-Zn alloy [1]. A recent study suggests the potential for using these alloys in applications that need elevated temp. Because RE may be mixed with mg either alone or in combination with aluminium and improves creep resistance measurements [1]. The researcher Xie et al. recorded a report on the effect of adding rare elements such as (Y, Nd) on the microstructure and mechanical properties of AZ81 alloy. One of the results is that adding rare elements with renewable energy works to soften the grains and form the Al_2Nd , Al_2Y phases. The studies of Xie et al. exhibit the advantage of the combined RE elements, but their works are not comprehensive enough. In Xie's work, the addition of Y and Nd is in a fixed ratio (w(Y)/w(Nd)=3:2), which means that the content of Y synchronously changes with Nd, Y synchronously with Nd, so it is difficult to discuss the interaction of different rare elements. In another paper, the neodymium component was fixed, and Gd was added in different proportions to AZ80 alloy to modify and improve its properties [2, 3]. Usually, trace elements are added to the Mg-AL alloy to prevent or hinder the formation of the $Mg_{17}Al_{12}$ phase during solidification because aluminium prefers to react with the trace elements RE to form the Al-RE phase between the metals. The addition of trace elements to the Mg-Al alloy leads to the formation of the Al_2RE, $Al_{11}RE_3$ phases in two phases. However, the thermodynamic stability of the Al_2RE phase is less stable than the $Al_{11}RE_3$ phase formed when temperatures rise above 150°C, where both Al_2RE and Al combine to form the $Al_{11}RE_3$ phase. After the transformation of the length to form another phase, which results in a deterioration in the mechanical and corrosion properties when the temperature rises [4-6]. Hence, the importance of adding an alternative that can improve or maintain the properties of the Mg-Al alloy when temperatures rise, and neodymium can be an effective element added to magnesium alloys for high-temperature applications. [7]. Neodymium is one of the most stable metals with aluminium and thus restricts the formation of phases. The authors in [8] investigated the effect of ageing time on the Vickers hardness of Mg-4Al-4Nd-0.5Zn-0.3Mn alloy stated that the forms of the formed phases (Al2RE, Al-11RE3) change their shape from polyhedron and long rod shape to small rod-like granular sediments respectively under T6 conditions, because of these deposits resulting from the heat treatment leads to an improvement in the properties, hardness and yield resistance of the alloy at room temperatures and high temperatures. Therefore, AE alloys are challenged to meet the requirements of these components to obtain mechanical properties at temperatures above 150°C considerable protection from erosion, too. The impact of the RE effectiveness as a strengthening component on Magnesium-aluminium-based alloys generated by mechanically melted alloying and metallic mould pouring [9, 10].Currently, it is widely observed. None of the studies indicated applications in which neodymium is added to the Mg-Al alloy and its effect on in vitro corrosion. This article is concerned with preparing a new magnesium alloy used in the medical field as a biodegradable alloy and studying its mechanical properties and corrosion behaviour in a biological solution.

MATERIALS AND METHODS

Materials and sample preparation

The materials used in the research are pure magnesium of purity (99.9%) obtained from the mineral madencilik/turkey, pure aluminium of purity (97.9%) obtained from murat geri Dönüşüml turkey, and pure Nd of purity (98.8%) were obtained from china. The new alloy (Mg-2%Al-1%Nd) was prepared by the investment casting method. 750 C° of mg was heated in a crucible vessel employing an electromagnetic durability combustion chamber, and the required temperature was maintained for 45 minutes; at this temperature 2%aluminum and 1% Nd were added to the melt for modifications, respectively. The molten is poured into a mould of gypsum prepared by the 3D Printer, then poured by bottom pouring arrangements into a preheated (200 C°), and placed in a device to empty air bubbles and remove them from the molten at a pressure of 1 mbar. It is poured into a protective atmosphere of SF6 (1%, v/v) and CO_2 (Bal). After the solidification process is completed, it is washed with distilled water to remove the gypsum mould and the alloy is extracted as shown in Figure 1. Then, a solution treatment was carried out for homogenizing at

(a) (b)

Fig. 1. Photo of specimen (a) the ingot, (b) after cutting

350 C° for a period of 2 h, followed by cooling or quenching with water at room temperature [11], and finally, cutting the alloy using (wire cutting) into disc specimens with a diameter of 12mm and a height 3 mm Table 1 showed the codes of the specimens in this study.

Microstructure characterization

The X-ray fluorescent determined the chemical compositions of the casting alloy (AN21) were conducted as in Table 2, which shows the chemical composition of the casting alloy.

The metallographic specimens were cut, mechanical grinding with sic paper at a grad (800, 1200,2000), then washed with distilled water, dried well, and cleaned with acetone using ultrasonic cleaning for 5 min, then became ready for subsequent tests. Chemical etching in a solution consisting of (100 ml ethanol, +20 ml distill water, +12 gr picric acid, and +6 ml acetic acid) was achieved for 10–20 s [4, 12]. An XRD analysis was performed to determine the occurring phases. It was carried out on ((Shimadzu, XRD-7000, and Japan) for all specimens before and after heat treatment. The measurement settings were: Cu target at 30 mA and 40 kV, scanning speed of 2 deg/min for scanning range of 10–80°. The microstructure of the base alloy was investigated using a scanning electron microscope (SEM) (TESCAN and Model: VEGA3SBH). Energy-dispersive spectroscopy (EDS) was used to know the existence of elements in the fabrication of the samples. Analysis was performed on the specimens to know the existence of different phases.

Table. 1. The codes of specimens and description

Codes of specimens	Description
B	Mg-2Al-1Nd alloy without annealing
C	Mg-2Al-1Nd alloy with annealing

Mechanical properties

Micro hardness test

Vickers' microhardness test was used to evaluate the microhardness of the B and C alloys. A square-based diamond indenter was used to apply a weight of 100 g to the test specimen for 10 seconds, and standard hardness readings were taken [13]. The experiment was conducted three times for each specimen, and the average of the results was recorded.

Compression test

Compressive properties are evaluated using UTM (INSTRON-E1025) with a strain rate of 1 mm/min .Compression testing specimens were prepared as per ASTM: E9 standard [13]. It is possible to know the value of the elastic modulus of the alloy from stress-strain curve; a load was applied to a cylindrical sample with dimensions: 12 mm diameter, and 10 mm height, shown in Figure 2.

Table. 2 Chemical composition of AN21 alloy

Element	Mg	Nd	Al	Si	S	Cl	K	Ca	Mn	Fe	Ni	Zn
Wt%	96.427	1.218	2.094	0.0398	0.0444	0.0593	0.0164	0.0232	0.0466	0.0126	0.0095	0.079

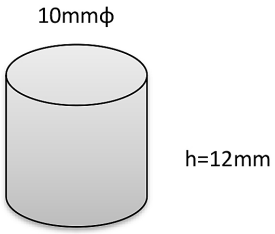

Fig. 2 ASTEM stander of compression test

Corrosion behavior

Electrochemical measurement

Both potentiodynamic polarization (PDP) and electrochemical impedance spectroscopy (EIS) were carried out. All the tests were performed in a typical three-electrode cell with a three-electrode configuration utilizing the potential dynamic polarization (PDP) test and the open-circuit potential (OCP) test in SBP solution with a pH value of 7.2 and at 37 °C. A platinum plate with an area of 1.13 cm^2, a saturated calomel electrode, and the sample with an exposed area of 1.13 cm^2 served as the counter electrode, reference electrode (RE) and working electrode (B and C) alloy. To ensure a steady state of alloys, a short-term OCP test was carried out for 1h before the potential dynamic polarization test. After the OCP test, PDP measurement was performed from -220 mV (OCP of each sample). Also be used equation (1) to estimates of corrosion amounts,The equation was used to define the corrosion rate based on ASTM G102 [14, 15].

$$CR = (k \cdot I_{corr} \cdot EW)/\rho \tag{1}$$

where: CR – the corrosion rate (mm/y), k = 3.27×10^{-3} mm/g, ρ – the density of magnesium alloy, I_{corr} – the current density, EW – equivalent weight.

The EIS data were fitted by Zview software (Scribner Associates, Inc., NC, USA) and polarization curves were fitted by Nova software (Metr ohm CO., Ltd., CH). From the Tafel curves, the corrosion resistance of each group was obtained as per the ASTM standard G102. The corrosion potential and current density were calculated by the Tafel extrapolation method. One of the most important objectives of this article is to test the corrosion of this alloy in a simulated blood plasma solution consisting of [6.8 NaCl, 0.1$MgSO_4$, 2.2$NaHCO_3$, 0.216Na_2HPO_4, 0.026 NaH_2PO_4, 0.2 $CaCl_2$ and 0.4KCl, and deionized water] as g/l [4]. A corrosion behaviour test using the potential dynamic polarization (PDP) method was conducted for specimens B and C to identify the effect of the homogeneous distribution of phases and defects in the base alloy on corrosion resistance. EIS TEST was measured via an operating frequency range of 100 kHz to 50 MHz and a change in intensity of 10 mV (OCP after 1h). Gamry Echem Analyst software (Gamry Instruments, Inc.) was used to evaluate and fit EIS data to powered equivalent circuits, and the polarization resistance (Rp) was determined via the fitting equation below:

$$Rp = \frac{\beta a \times \beta c}{2.3 Icorr[\beta a + \beta c]} \tag{2}$$

Simultaneously following the EIS tests, the potentiodynamic studies occurred, commencing from 0.2 V to + 0.6 V versus OCP, with an average scan rate of 1 mV/s [16].

Immersion or Mass loss method

The simplest way of evaluating materials that are degrading is mass loss measurements. According to ASTM-G31-72, the mass loss of the immersed sample is utilized to calculate the degradation rate. Measured the weight of the specimen before and after 1, 3, 5, 8, and 10 days of the immersion test. The deterioration layer may be removed more easily, and the degraded surface can be seen after chromatic acid treatment (180 g/l and 2 g/l $AgNO_3$ in distilled water). Following is how the deterioration rate was estimated.

$$MR = \frac{\Delta m}{S\ t\ \rho} \tag{3}$$

where: MR – the degradation rate, Δm – the mass loss, S – the original surface area exposed to the corrosive media, t – the exposure time, ρ – the standard density [17].

In vitro bioactive test

The specimens were immersed in an SBF in accordance with the standard BS ISO 23317:2007[18],to assess the bioactivity of Mg-2Al-1Nd alloy both before and after annealing. The elements of the solution required to create the SBF solution are shown in Table 3. The B and C alloy were then placed in a vessel containing SBF before being submerged in water for six hours. The pH and beginning temperature of the SBF were 7.4 and 37 °C, respectively. The specimens were carefully washed via ionized water after six hours and then dried at 37 °C in preparation for

Table 3. Chemical composition of SBF used in this paper [20]

Order reagent amount (g)	Order reagent amount (g)	Order reagent amount (g)
1	NaCl	8.035
2	$NaHCO_3$	$NaHCO_3$ 0.355
3	KCl	0.225
4	$K_2HPO_4 \cdot 3H_2O$	0.231
5	$MgCl_2 \cdot 6H_2O$	0.311
6	c(HCl) = 1 mol/l	39
7	$CaCl_2$	0.292
8	Na_2SO_4	0.072
9	TRIS	118
10	c(HCl) = 1 mol/l	0 to 5

analysis. After the bioactivity test, SEM and EDX investigations were carried out to look into the specimens› bioactivity behaviour [19].

RESULTS AND DISCUSSION

XRD and microstructure

The X-ray diffraction pattern of the cast alloys B and C is shown in Figure 3. Peaks in (Mg17Al12) and α-Mg identify the Mg-2Al alloy. The phase was completely suppressed when one weight per cent Nd was added to the Mg-2Al alloy and peaks of the α-Mg and Al_2Nd phases appeared instead. Figures 3 and 4 show the phases formed Al_2Nd, AlNd intermetallic phases in alloy after the addition of Nd, by the SEM Test, which gives results confirming the results of the XRD test in Figure 5, where the existing phases appear in different shapes as shown in the figure and with different magnification forces to illustrate the change of shapes after the homogenization process. Since it is well known that the likelihood of a compound

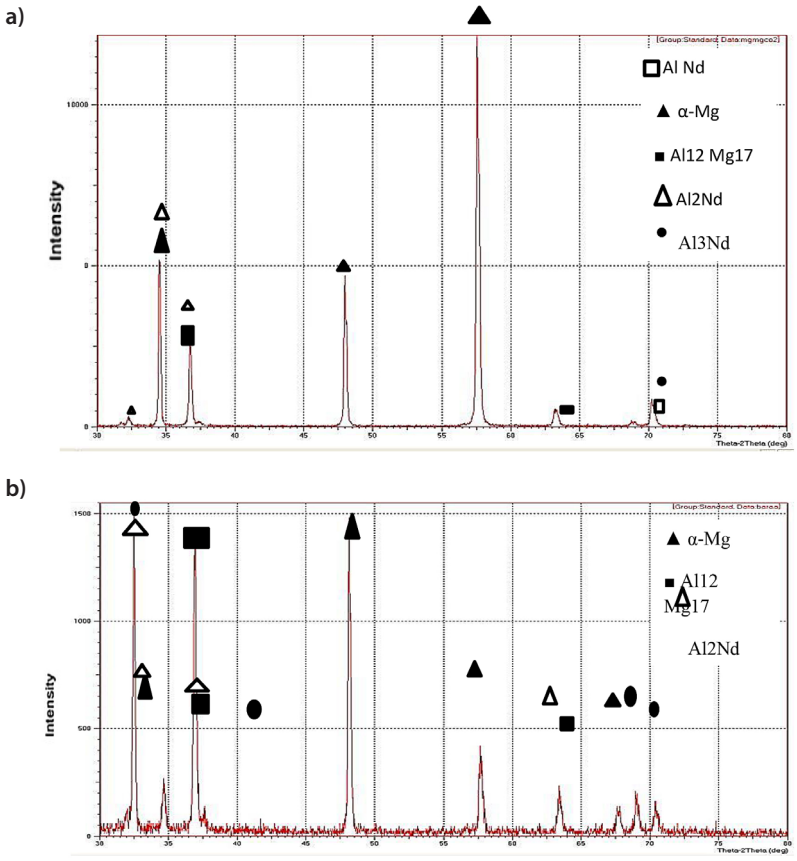

Fig. 3. XRD pattern for: (a) B alloy and (b) C alloy

forming between two elements depends on the difference in their electronegativity, the creation of intermetalic could be explained by taking note of the electronegativity of the elements. Nd, Mg, and Al have electronegativity values of 1.14, 1.61, and 1.31, respectively. Here, it is evident that the electronegativity difference between Nd and Al is bigger than that between Mg-Nd and Mg-Al, which caused the creation of Al-Nd intermetallic. The intermetallic of Al and Nd formed at a considerably higher temperature than the phase. Hence, the Al-Nd phases solidified before the latter in the solidification sequence [4, 21].

HARDNESS TEST

The phases mentioned in the previous (Al_2Nd) and (AlNd) are responsible for improving and increasing the hardness of the prepared alloy, as we notice a very clear improvement in the hardness values, especially after performing the homogenizing treatment, where the phases are distributed in the base in a more homogeneous manner, which leads to a decrease or decrease in the presence of defects for the prepared alloy, in the current work have been the results of hardness test illustrated in Figure 6, as the amount of improvement in hardness, also homogenizing treatment, in a short period and without artificial ageing, decreases for long periods with ageing and high temperatures that lead to the formation of large pores, which is a reason for the decrease in hardness.

Compression test

From the resulting stress-strain diagram in Figure 7, it is possible to know the value of the elastic modulus of the alloy, and its value is very close to the elasticity modulus of the bone of a human being. The reason is the presence of elements such as neodymium and aluminium, which give flexibility to the prepared alloy, in addition

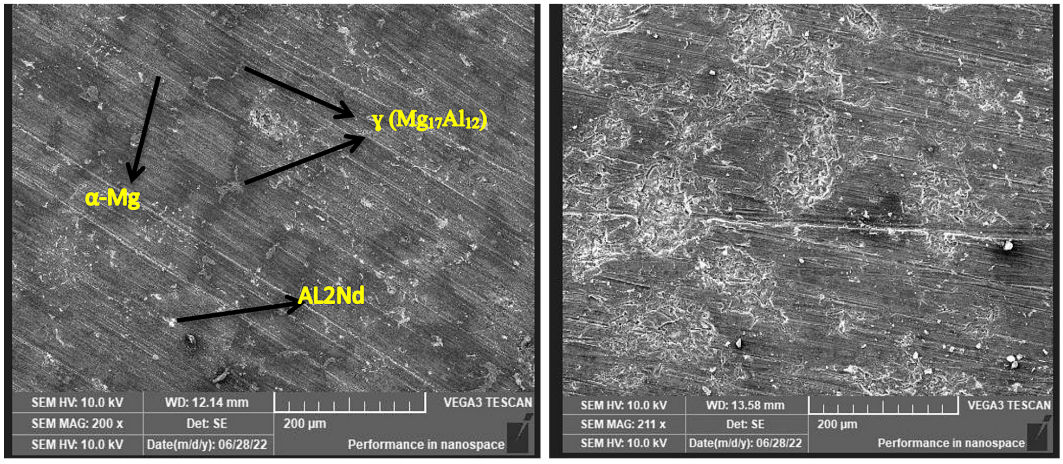

Fig. 4. SEM image of B and C specimens with magnification 200X

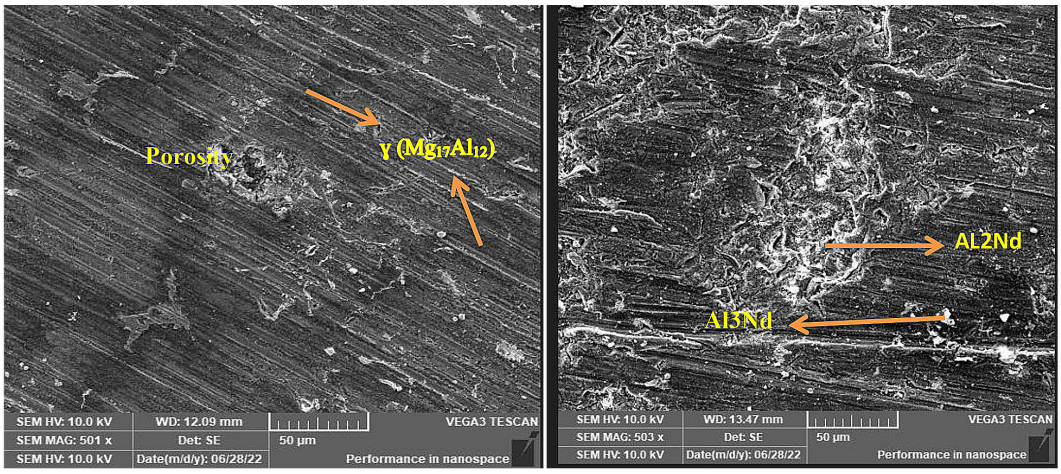

Fig. 5. SEM image of B and C specimens with magnification 500X

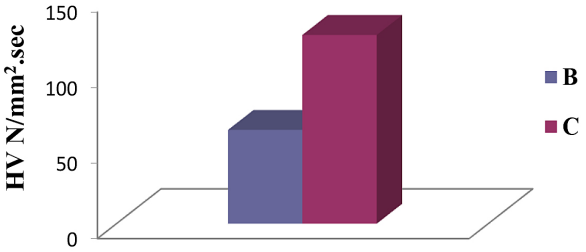

Fig. 6. The improvement of hardness values

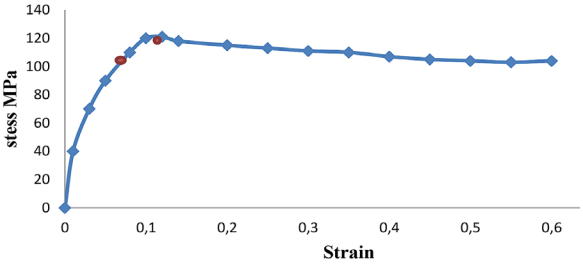

Fig. 7. Stress-strain curve of treated alloy

to High compressive strength [22] and low density, as shown in Table 4, which represents a comparison of properties and Figure 7, which represents the stress-strain curve of the prepared magnesium alloy.

The mechanical properties of Mg-Al-Nd biodegradable alloys can be improved by heat treatment. Heat treatment can cause the precipitates to grow larger and more coherent, further hindering dislocation movement. In addition, heat treatment can also cause the formation of new precipitates, such as Mg_2Nd, which are even stronger than the Al and Nd precipitates. Overall, the compression stress-strain curve for Mg-Al-Nd biodegradable alloys is characterized by a linear elastic region followed by a plastic deformation region. The yield strength, ultimate strength, and strain at failure of the alloy can be improved by heat treatment [24].

Corrosion behavior in SBP solution

Electrochemical tests

The anti-corrosion properties of the B and C specimens are evaluated by potentiodynamic polarization tests. Figure 8a shows the Tafel curve of alloys in simulated blood plasma solution. The corrosion potential (Ecorr) and corrosion current density (icorr) were determined using the Tafel extrapolation method, and the polarization resistance values (Rp) were calculated based on the Sterne-Geary formula given by Eq. (2), where βa and βc are the anodic and cathodic Tafel slopes, respectively. The corresponding Tafel data are summarized in Table 5. In general, more positive Ecorr is regarded as the proof for better anti-corrosion performance of alloys. It can be seen from Fig. 8a that the C alloy enhanced the Ecorr compared with the B alloy, which could be a good indication of the surface stability[19]. The corrosion resistance increases and the corrosion rate decreases. The polarization resistance values of the C sample (Table 5) increase after annealing. Also, Fig. 8b shows the identical electricity circuits of the B and C alloys and each of their EIS Nyquist charts during 1 h of being exposed to the physiological fluid. In simulating blood plasma solution, the Nyquist plots show capacitive loops at high and medium frequencies. The approximate resistance for every electricity loop, Rt for the SBP solution, R1

Table 4. Physical and mechanical properties of biomedical magnesium and some magnesium alloys in comparison with natural bone [23]

Properties	Natural bone	Mg cast	AZ91 die-cast	AZ31	C alloy ours
Density (g/cm^3)	1.8-2.0	1.74	1.81	1.78	1.72
Compression strength (MPa)	164-240	--	160	60-70	104
Elastic modulus (GPa)	5-23	41	45	45	42
Yield strength (MPa)	104.9-114.3	20.9-2.3	150	125-135	110
Ultimate tensile strength (MPa)	35-283	86.8	230	235	120.2

Table. 5 Improvements of the corrosion parameters [potential energy (E), current density (I), corrosion rate (C.R) and polarization resistance (R_p)] of B and C alloy after immersion time in SBP at 37°C

Samples	E potential energy [mv]	βa	βc	I_{corr}[mA·cm^{-2}]	Rp KΩcm^2	C.R mm·y^{-1}
B	-1340.3	46.9	-46.6	1.445	0.07	3.37
C	−1450	56.1	-101.9	0.038	4.13	0.089

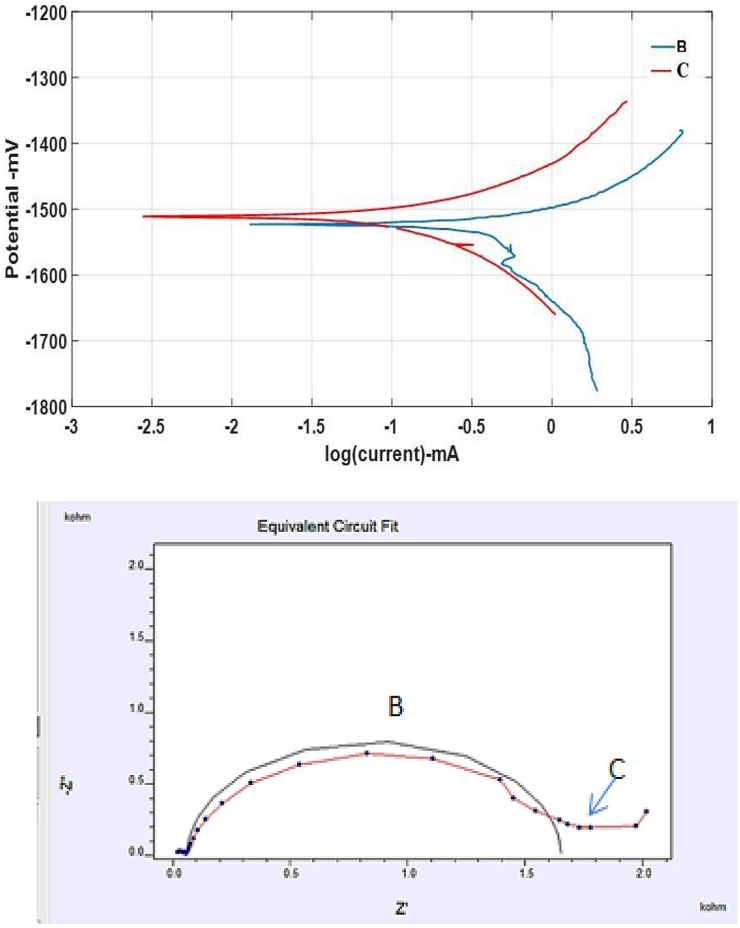

Fig. 8. Electrochemical corrosion result: (a) potentiodynamic polarization (PDP), (b) Nyquist spectra plot of 1h samples recorded at OCP after soaking in simulated blood plasma

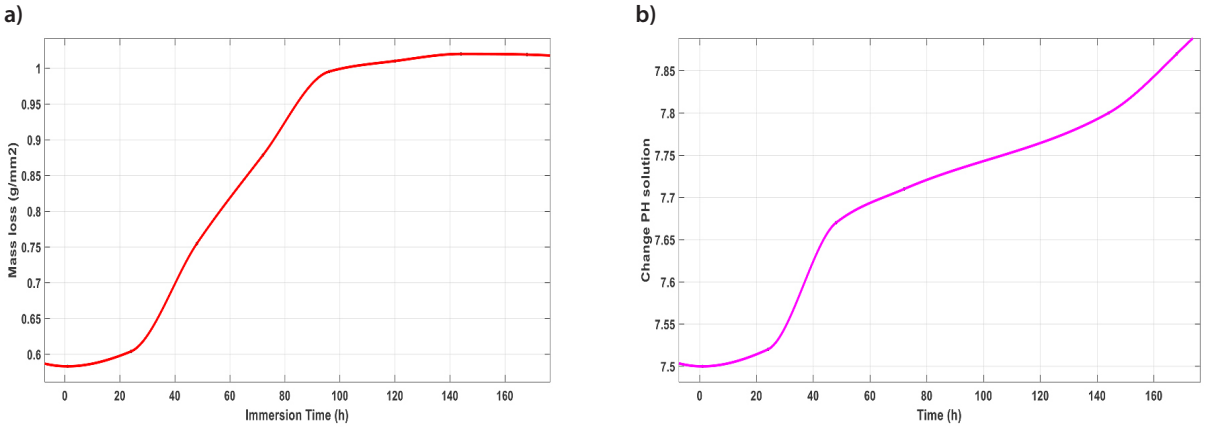

Fig. 9. The degradation rate of alloys by: a) weight loss of the C alloy after immersion in the Simulated blood plasma solutions for 1 to 10 days, (b) pH value change of specimen

+ R2 may be calculated to obtain the Rt values from the EIS data. The behavior predicted by the descriptive evaluation of the half-circle diameters in the Nyquist graphs is supported by the Rt values shown in Figure 8b.

Degradation rate calculation by mass loss

Deterioration rate in static circumstances, indicating a ratio limit A decrease in the solubility of substances that will conform the degradation layer under simulated physiological solutions

(such as $Mg(OH)_2$, $MgCO_3$, $CaCO_3$, $Mg_3(PO_4)_2$, or $Ca_5(PO_4)_3$) is promoted by the alkalization of the surface environment (OH). The passivation of the magnesium surface in alkaline conditions is brought on by this decrease in solubility, which precipitates oversaturated compounds as a degradation layer. When a low V/A ratio is used, this alkalization process should be considered even for buffered degradation mediums [25]. Deterioration rate in static circumstances, indicating a ratio limit Limitations on the surface-based diffusion of buffering species and OH are brought about by the static circumstances, which also cause the buffer capacity to depend on the volume of the buffer. The chosen V/A ratio used in static in vitro tests should be stated for the reasons mentioned above to make comparisons across trials easier [19]. The ASTM G31-72 indicates that the chosen V/A ratio should be high enough to prevent the medium from becoming alkaline over the planned immersion time indicated in Fig.9 explained improvement in degradation rate which calculated from Eq. 3 the degradation rate have become 1.045 g/mm^2 for 10 days.

In vitro bioactive test

Figure 10 shows the XRD diffraction patterns for new Mg alloys treated, after 1-5 days of exposure in simulated body fluid solution. The spectra suggest the presence of hydroxyapatite (HA) on the alloy studied. In contrast, the HA peaks in the C alloy appear more prominent than in the B alloy. It may be due to variations in the position of the apatite or the growth of a thicker film of HA on treated alloys as opposed to untreated ones. Several researchers however have determined that this apatite is composed of Ca10.00P6.00O26.00H2.00. [20, 26]. Further, Figure 11 shows the change in the. An in vitro evaluation of bioactivity or apatite formation in simulated body fluid can be used to predict the bioactivity behaviour in vivo.

CONCLUSIONS

This work included preparing a novel magnesium alloy as a degradable biomaterial and studying its properties and corrosive behaviour in biological media. Among the most important conclusions that were reached are included in the following paragraphs:

- Investment casting is an effective method of manufacturing new magnesium alloy.
- Homogenizing treatment improves the mechanical properties of hardness and reduces crystal defects within the substructure, leading to an increase in the hardness values and an improvement of 75% and comparison strength improvement values of 47.80%.
- The prepared alloy's elastic modulus and density make it one of the closest magnesium alloys to the properties of human bone.
- The degradation rate has been improved by 1.045 g/mm^2 for an immersion time of 10 days.
- The corrosion resistance of this alloy after immersion in simulated blood plasma (SBP) solution improves after performing the homogenization treatment to have corrosion rate values of 0.897 mm/y. Thus, it has proven successful

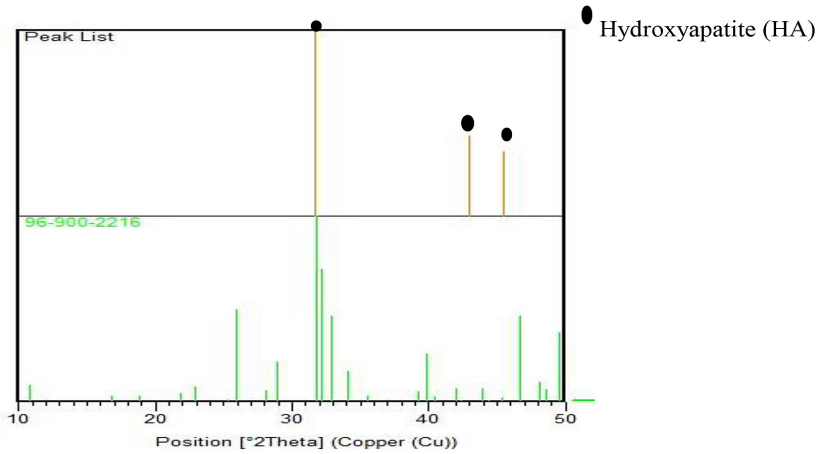

Fig. 10. XRD diffraction patterns of alloys after 5 days of immersion in SBF solution

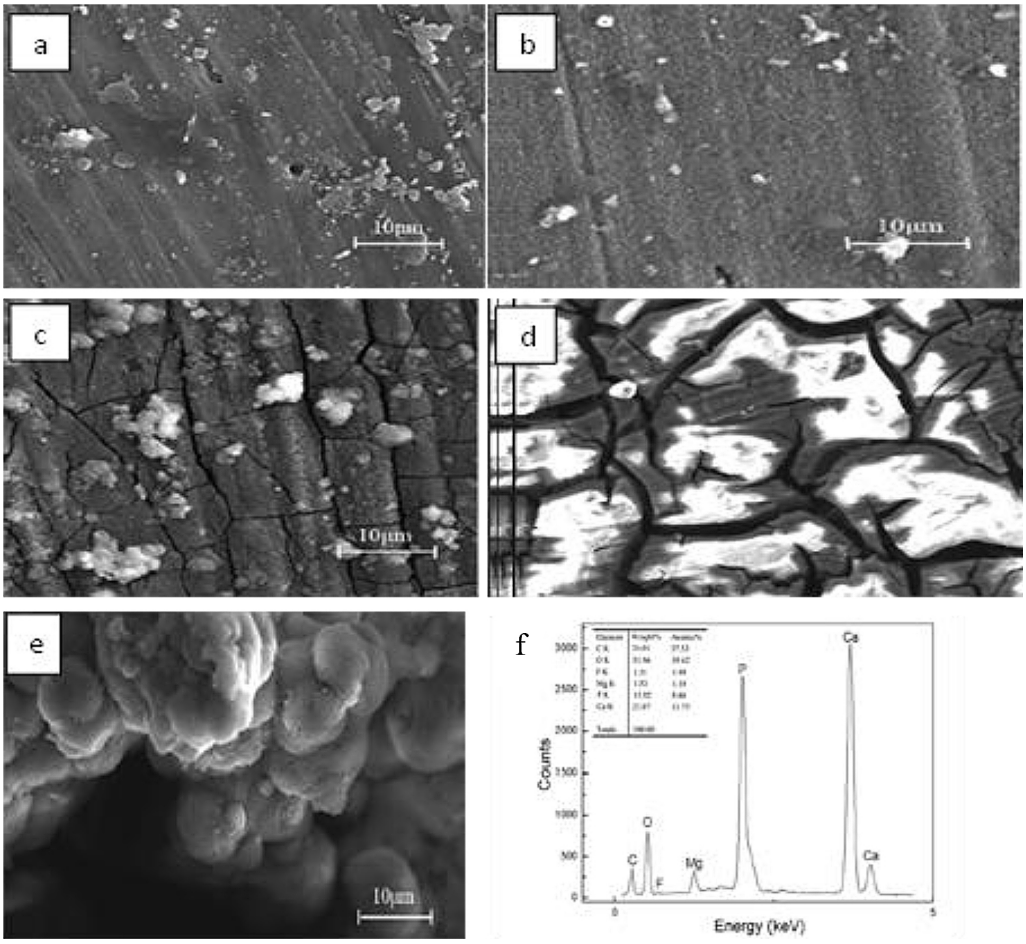

Fig. 11 SEM of C alloy after immersion in SBF (1-5) days: (a) formation HA on surface of specimens after immersion 1day ,(b) after immersion 2 day ,(c),(d),(e) after immersion 3-4-5days respectively ,(f) EDS for the specimens immersion 5 day explain chemical composition of the surface after immersion in SBF for 5 days

in its resistance to corrosion in vitro and excellent corrosion resistance in biological media.

- A new magnesium alloy in SBF degrades at a remarkably rapid pace. The most significant result in this study is that Mg has shown to be a highly bioactive material that generates an apatite layer on its surface after only 5 days of immersion in SBF, albeit it can be reduced by previously heated specimens. This suggests that magnesium can be exploited as a source of magnesium ions in biomimetic processes or as a bioactive component in the creation of materials for tissue regeneration.

REFERENCES

1. Bettles C.J., Moss M., and R. Lapovok, A Mg–Al–Nd alloy produced via a powder metallurgical route, Materials Science and Engineering: A, 515(1-2), 2009, 26-31.
2. Jiang N., Lei C., Linggang M., Canfeng F., Hai H., Zhang X., Effect of neodymium, gadolinium addition on microstructure and mechanical properties of AZ80 magnesium alloy, Journal of Rare Earths, 34(6), 2016, 632-637.
3. X. Wang, Y. Lin, Z. Liu, and S. Liu, Improving mechanical properties of a cast Al–Mg alloy with high Mg content by rapid solidification, Materials Science and Engineering: A, 2022, 852, #143709.
4. S. Mishra, A. Chaubey, and A. Mandal, Effect of heat treatment on the microstructure of Mg-4Al-Nd alloys, Technologies, 2017, 5(2), 23. doi: https://doi.org/10.3390/technologies5020023.
5. Moreno I., Nandy T., Jones J., Allison J., Pollock T., Microstructural stability and creep of rare-earth containing magnesium alloys,Scripta Materialia, 48(8), 2003, 1029-1034.
6. G. Gaurav and P. Chakraborty, Effect of annealing on the microstructure evolution of cold-rolled Mg-6Al-3Sn alloy, Materials Today: Proceedings, 2022.
7. Wang Y.-x., Fu J.-w., and Yang Y.-s., Effect of Nd addition on microstructures and mechanical

properties of AZ80 magnesium alloys, Transactions of Nonferrous Metals Society of China, 22(6), 2012, 1322-1328.

8. Feng L., Dong X., Cai Q., Wang B., Ji S., Effect of Nd on the Microstructure and Mechanical Properties of Mg-La-Ce Alloys at Ambient and Elevated Temperatures, Journal of Materials Engineering and Performance, 2022, 1-9.
9. Somasundaram M., NarendraKumar U., Microstructural and Mechanical Properties of a Heat-Treated EV31A Magnesium Alloy Fabricated Using the Stir-Casting Process, Crystals, 12(8), 2022, 1163.
10. Zhang J. et al., Effect of Nd on the microstructure, mechanical properties and corrosion behavior of die-cast Mg–4Al-based alloy, Journal of Alloys and Compounds, 464(1-2), 2008, 556-564.
11. Nouri M., The Effect of Yttrium on Wear, Corrosion and Corrosive Wear of Mg-Al Alloys, 2017.
12. Liu X. et al., Effect of carbon interface on adhesion and anti-corrosion properties of hydroxyapatite coating on AZ31 magnesium alloy, Materials Chemistry and Physics, #126351, 2022.
13. Veeranjaneyulu I., Chittaranjan Das V., and Karumuri S., Enhancing the Mechanical Properties of AZ31D Alloy by Reinforcing Nanosilicon Carbide/Graphite, Journal of Nanomaterials, vol. 2023.
14. Astm G., Standard practice for calculation of corrosion rates and related information from electrochemical measurements, G102-89, 2004, doi: 10.1520/G0102-89R15E01
15. Shinde S. and Sampath S., A Critical Analysis of the Tensile Adhesion Test for Thermally Sprayed Coatings, Journal of Thermal Spray Technology, 31(8), 2022, 2247-2279. doi: https://doi.org/10.1007/s11666-022-01468-z.
16. Mena-Morcillo E., Veleva L., Degradation of AZ31 and AZ91 magnesium alloys in different physiological media: Effect of surface layer stability on electrochemical behaviour, Journal of Magnesium and Alloys, 8(3), 2020, 667-675.
17. Witte F. et al., In vitro and in vivo corrosion measurements of magnesium alloys, Biomaterials, 27(7), 2006, 1013-1018.
18. Da Silva C.G., Monteiro J.R., Oshiro-Júnior J.A., Chiavacci L.A., Hybrid Membranes of the Ureasil-Polyether Containing Glucose for Future Application in Bone Regeneration, Pharmaceutics, 15(5), 2023, 1474.
19. Bordbar-Khiabani A., Yarmand B., Mozafari M., Enhanced corrosion resistance and in-vitro biodegradation of plasma electrolytic oxidation coatings prepared on AZ91 Mg alloy using ZnO nanoparticles-incorporated electrolyte, Surface and Coatings Technology, 360, 2019, 153-171. doi: https://doi.org/10.1016/j.surfcoat.2019.01.002.
20. Sasikumar Y., Solomon M., Olasunkanmi L., and Ebenso E., Effect of surface treatment on the bioactivity and electrochemical behavior of magnesium alloys in simulated body fluid, Materials and Corrosion, 68(7), 2017, 776-790.
21. Cui X., Yu Z., Liu F., Du Z., and Bai P., Influence of secondary phases on crack initiation and propagation during fracture process of as-cast Mg-Al-Zn-Nd alloy, Materials Science and Engineering: A, 759, 2019, 708-714.
22. Zerankeshi M.M., Alizadeh R., Gerashi E., Asadollahi M., Langdon T.G., Effects of heat treatment on the corrosion behavior and mechanical properties of biodegradable Mg alloys, Journal of Magnesium and Alloys, 2022.
23. Heakal F.E.-T., Bakry A.M., Corrosion degradation of AXJ530 magnesium alloy in simulated pysiological fluid and its mitigation by fluoride and chitosan coatings for osteosynthetic applications, Int. J. Electrochem. Sci, 13(8), 2018, 7724-7747. doi: https://doi.org/10.20964/2018.08.67
24. Wang P., He W., Xu H., Phase Equilibria at 500ºC of the Mg-Nd-Zn System in the Region of 0-50 At% Nd. Available at SSRN 4484066.
25. Gerengi H., Cabrini M., Solomon M.M., Kaya E., Understanding the corrosion behavior of the AZ91D alloy in simulated body fluid through the use of dynamic EIS, ACS omega, 7(14), 2022, 11929-11938.
26. Topuz M., Hydroxyapatite–Al2O3 reinforced poly–(lactic acid) hybrid coatings on magnesium: characterization, mechanical and in-vitro bioactivity properties, Surfaces and Interfaces, 37, 2023, 102724.